Wall slip mechanisms in direct and inverse emulsions

X. Zhang, Elise Lorenceau, Tarik Bourouina, Philippe Basset, Thomas Oerther, Maude Ferrari, Florence Rouyer, Julie Goyon, Philippe Coussot

Wall slip mechanisms in direct and inverse emulsions

X. Zhang,[1] E. Lorenceau,[2] T. Bourouina,[3] P. Basset,[3] T. Oerther,[4] M. Ferrari,[5] F. Rouyer,[1] J. Goyon,[1] and P. Coussot[1,a)]

[1]*Univ. Paris-Est, Laboratoire Navier (ENPC-IFSTTAR-CNRS), 2 Allée Kepler, 77420 Champs sur Marne, France*
[2]*Univ. Grenoble-Alpes, CNRS, LIPhy, 38000 Grenoble, France*
[3]*Univ. Paris-Est, ESYCOM EA 2552, ESIEE Paris-CNAM-UPEM, 5 Bd Descartes, 77420 Champs sur Marne, France*
[4]*Bruker BioSpin GmbH, Silberstreifen 4, 76287 Rheinstetten, Germany*
[5]*Université de Lorraine, CNRS, LEMTA, 2 Avenue de la Forêt de Haye, F-54000 Nancy, France*

(Received 3 July 2018; final revision received 18 October 2018; published xx xx 2018)

Abstract

We carry out a series of experiments with the aim of completing our knowledge of wall slip characteristics, through a deductive approach based on macroscopic behavior observations. More precisely, we use model materials (direct and inverse emulsions) and determine the variations of wall slip properties depending on the material parameters (droplet size, concentration) and boundary conditions of the flow (free surface or flow between two solid surfaces, normal force, flow beyond yielding, and coated or rough surface). The wall slip characteristics are determined from long creep tests at different levels and from internal measurements of the velocity profile in the capillary or the Couette flow as determined by magnetic resonance imaging. First, we show that the slip yield stress is due either to edge effects in relation with evaporation then pinning around the line of contact or to a kind of adhesion of the suspended elements to the wall. This adhesion effect varies with the characteristics of the solid surface (interaction with elements, roughness), and wall slip (below the yield stress) disappears when the adhesion or adherence leads to a wall slip yield stress expected to be larger than the material yield stress. Then, we show that, below the yield stress, the slip velocity vs shear stress (from which the slip yield stress has been removed) relationship is linear. The corresponding value for the apparent slip layer made of interstitial liquid appears to be independent of the concentration and to vary only slightly with the droplet size. Moreover, it is independent of the normal force (below the critical value inducing elongation) and other experimental conditions, e.g., it is the same for free surface flows. Although the origin of this phenomenon remains to be found, the following scheme appears to be consistent with all observations: the droplets are attracted at a very short distance from the wall, forming regions of small area in which the liquid layer thickness is very small, the shear stress being dominated by the shear in these regions. Finally, this apparent layer thickness increases at the approach of the yield stress and beyond, or if a slightly rough surface is used, leading to a faster (quadratic?) variation of the slip velocity as a function of the stress. https://doi.org/10.1122/1.5046893

I. INTRODUCTION

Concentrated suspensions, which are yield stress fluids, flow only when submitted to a stress greater than a critical stress, called yield stress (τ_c) [1,2]. However, on smooth surfaces, they can move even under smaller stress, a phenomenon called wall slip. When it occurs, the bulk material moves as a rigid block for stress below τ_c, which defines a slip velocity V_S, but it has also been observed that some wall slip can still occur at larger stress [3,4]. Wall slip has a critical impact on rheological characterization since in that case the apparent flow does not reflect the bulk properties of the fluid. It may also play a critical role in various applications involving food [5], cosmetic [6], civil engineering [7,8], and biological [9] materials.

To gain quantitative insights into wall slip properties, it is usual to compare rheological measurements, obtained with smooth surfaces, with measurements under similar flow history but now with rough surfaces assumed to suppress wall slip. This, in particular, provides a straightforward measurement of the slip velocity for stress below the yield stress since in that case the bulk behaves as a rigid block so that the apparent relative motion of the rheometrical tools necessarily relates to a localized motion along the wall-material interface where the material structure, and thus its behavior, differs from that of the bulk. It is also possible to directly measure the slip velocity (by determining the velocity profile) using methods such as laser doppler velocimetry [10], digital image methods [11], ultrasonic velocimetry [12], magnetic resonance imaging (MRI) [13], and near-field optical methods [14]. The materials exhibiting wall slip include concentrated suspensions, soft particle suspensions, emulsions, and foams [15]. Power-law dependencies for stress vs. slip velocity are generally obtained but the exponent was found to vary from 0.5 to 1.

A few theories have been developed to account for the wall slip; they generally assume the shear of a thin liquid layer between the bulk material and the solid surface. To explain the wall slip behavior of soft particle suspensions, Meeker *et al.* [11,16] have developed an elastohydrodynamic theory for concentrated suspensions of soft (deformable) particles (e.g., microgels, emulsions). They consider that the

a)Author to whom correspondence should be addressed; electronic mail: philippe.coussot@ifsttar.fr

liquid layer separating soft suspended objects from the wall is maintained by the balance between the lubrication flow in the slip layer, which creates a lifting force that pushes the suspended particles away from the solid surface, while the elastic force induced by particle deformation and related to the osmotic pressure in the concentrated system tends to reduce the slip layer thickness. This approach basically leads to a quadratic dependence of the slip velocity with regard to the shear stress. A later work [17] completed this theory by considering various short-range interactions between the first layer of the soft particles and the solid surface. In the case of the dry foams, Denkov *et al.* [18] proposed the shear stress to depend on a sum of two terms involving the wall slip velocity at different powers. This expression has later been revised by Le Merrer *et al.* [19].

In the case of hard sphere suspensions, Ballesta *et al.* [20,21] performed a detailed analysis of rheological data and showed that the relationship between the shear stress and the slip velocity is an affine function with a constant term corresponding to the residual stress τ_c', beyond which wall slip is apparently observed to occur. The existence of this wall slip yield stress had in fact been remarked in previous works with other material types, in particular, emulsions [22] and microgels [11]. However, it was reckoned that the physical origin of τ_c' is unclear [11,20,22]. It seems indeed somewhat contradictory to have both wall slip *a priori* associated with the shear of some liquid layer covering the wall and a constant stress term *a priori* associated with some kind of friction of the elements in contact with the wall. Recently, Zhang *et al.* [23] showed that if τ_c' is considered as an edge effect and removed from the stress to get the flow curve strictly associated with wall slip, then a linear wall slip law applies to a wide range of systems, similar to previous results for hard sphere suspensions [20,21].

The fact that such a general behavior is obtained for different material types (soft or hard particles, plateletlike, or rounded particles) and structures (large or small porosity) suggests that some generic origin of wall slip should be sought, but this seems rather challenging. At first sight, it is natural to consider that such a result corresponds to the hydrodynamic lubrication regime proposed by Meeker *et al.* [16], associated with a constant thickness (δ) of lubricating liquid layer. However, for such different materials, we hardly see what could be the origin of this regime and how it could lead to similar values for δ. In fact, the existence of a uniform and constant liquid layer separating the bulk and the wall is difficult to support if we consider that the bulk is a heterogeneous material made of elements forming a jammed, disordered structure; such a structure is necessarily rough, with a roughness of the order of the element size, and thus, in general much larger than δ (at least for the above listed material types). As a consequence, we rather expect that this rough structure would tend to approach the wall at the closest possible distance. The question now is why we still get some apparent wall slip under such conditions. For emulsions, Princen [22] considered that there always remains a thin liquid layer between suspended droplets and a solid wall, which would result from various repulsive and attractive forces, but did not provide more explanation. Recently, Le Merrer *et al.* [19] provided a detailed approach of this problem, considering that this layer results from a balance between the osmotic pressure (due to capillary forces) in the foam and repulsive van der Waals and electrostatic forces. They, thus, estimated the value of δ between 5 and 50 nm.

Here, we carry out a further exploration of wall slip characteristics, which might provide further elements toward the understanding of the origin of wall slip. Since a direct view of the phenomena at the scale of the liquid layer along the wall, i.e., the ideal solution, is extremely challenging, our approach will be essentially macroscopic and deductive, relying on precise characterization under various conditions. More precisely, we will carry out different types of experiments with model systems to observe the variations of wall slip properties depending on material parameters (droplet size, concentration) and boundary conditions of the flow [free surface or flow between two solid surfaces, normal force, flow beyond yielding, coated surface, "intermediate" rough surface (not much larger than the particle size)]. In this frame, we will rely either on systematic creep tests at different levels or on internal measurements of the velocity profile in the capillary or the Couette flow as determined by MRI. Finally, the physical mechanisms at the origin of wall slip, seen as the interaction between the rough bulk and the wall, will be reanalyzed in the light of these results.

II. MATERIALS AND METHODS

A. Emulsions

First, we used oil-in-water (direct) emulsions with two different compositions: composition A has silicone oil (viscosity 0.35 Pa s) as dispersed phase and a continuous phase (viscosity 5 mPa s) made of 48.5 wt. % distilled water, 48.5 wt. % glycerol, and 3 wt. % myristyltrimethylammonium bromide (TTAB, Sigma-Aldrich); composition B contains dodecane oil (viscosity 1.36 mPa s) as dispersed phase and a continuous phase made of distilled water with 3 wt. % sodium dodecyl sulfate (SDS, Sigma-Aldrich). In addition, we used water-in-oil (inverse) emulsions at different water concentrations; 150 kg of $CaCl_2$ per cubic meter of water was added; the corresponding ions are dispersed in the droplets in a nonhomogeneous way, which induces some electrostatic field and finally, some repulsion between the droplets covered by the nonionic surfactant, which further contributes to stabilize the emulsion; the continuous phase is a dodecane oil with 7.5 wt. % of Span 80 (a commercial mixture of long chain sorbitan esters, including sorbitan monooleate). The preparation methods were similar to those used in previous works [24,25]. Two emulsifiers were used to prepare the emulsions. The first one is a Couette emulsifier (only for composition A), with a 100 µm gap between stator and rotator and a relative rotation velocity up to 600 rpm, inducing a shear rate of 16 200 s^{-1}. A Silverson mixer (model L4RT), equipped with a rotating steel blade inside a punched steel cylinder, was also used as the emulsifier. During the preparation, the fluids are sheared and the oil phase is broken into small droplets while the water or water/glycerol phase fills the surrounding environment, and the interface is stabilized by surfactants (TTAB and SDS). For composition

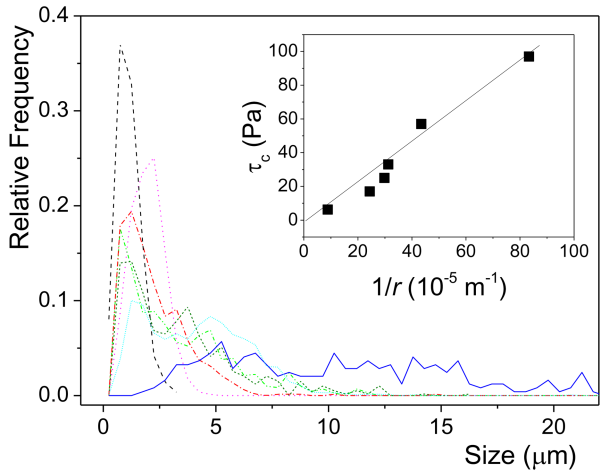

FIG. 1. (a) Droplet relative frequency as a function of size for emulsions made either with a Couette emulsifier at different rotation velocities: A1a, 600 rpm (light green dash dot dot), A1b, 600 rpm (dark green short dash), A2 300 rpm (light blue short dot), A3 150 rpm (dark blue) or with a Silverson emulsifier: A4 6000 rpm (black dash), A5 2400 rpm (red dash dot), B 6000 rpm (magenta dot). The oil concentration of the emulsions is 82 vol. %. The mean droplet sizes and polydispersities for these emulsions are A1a, 3.2 μm, 0.8; A1b, 3.4 μm, 0.7; A2, 4 μm, 0.6; A3, 11 μm, 0.8; A4, 1.1 μm, 1.6; A5, 2.3 μm, 0.7; B, 2 μm, 0.4. The inset shows the yield stress of each material as a function of the inverse of the mean droplet size for the same composition (A1–A5).

A (at an 82% oil volume concentration), the rotation velocity of the rotator (for the Couette emulsifier) or the rotating blade (the Silverson emulsifier) were varied (see Fig. 2) to obtain emulsions (named A1 to A5) with different mean droplet sizes. Note that the final emulsion characteristics are also dependent on other parameters such as the time of shear and the exact sample volume so that we could not precisely control the droplet size distribution (around the mean value): two emulsions A1 prepared through the same protocol may lead to slightly different droplet size distributions (see Fig. 1). For direct emulsions of composition B and inverse emulsions at different concentrations of the suspended phase (from 72% to 92% for composition B and 72% to 86% for the inverse emulsions), we only used the Silverson emulsifier at 6000 rpm. The characteristics of these different materials are also recaped in the Appendix.

To characterize the droplet size distribution, we used images of diluted emulsion samples captured with a confocal microscope and evaluated the particle size histogram with the software ImageJ. From the size distribution, we calculate mean droplet radius, r, and polydispersity (i.e., sqrt[mean(-size^2) – mean^2(size)]/mean(size)) (see Fig. 1). Although the distributions are not similar, there is a clear variation of the mean radius. In the inset of Fig. 1, the yield stress value of each emulsion is shown as a function of the inverse of the mean droplet size. It appears to follow a linear relationship, which is in agreement with the theoretical prediction of Princen and Kiss [26].

B. Surfaces

Different surface types were used for rheometry and inclined plane tests. Smooth silicon wafers are single side polished single-crystalline silicon wafers (Si-Mat). These surfaces are extremely smooth, with a root mean squared roughness (from the mean surface level) smaller than 0.3 nm, which is in the order of a single atomic silicon monolayer. This roughness was measured by atomic force microscopy [27]. This surface is later named "smooth surface." As silicon oxidizes itself naturally when exposed in air, parts of the surface may have become SiO_2.

A Teflonlike surface produced on top of a silicon wafer is also prepared by depositing a fluorocarbon thin film layer on the polished side of silicon wafers. Such a fluorocarbon thin film coating was produced by exposing the silicon surface for 20 s to a plasma of C_4F_8 under a flow rate of 200 cm^3/min, a pressure of 20 Pa, and a radio-frequency source power of 1800 W with bias power of 10 W. The resulting Teflonlike thickness is in the order of 100 nm. The plasma process resulted in a conformal deposition with no observable roughness under scanning electron microscope (SEM) and under interferometric optical profiler, which led us to the conclusion that it is much below 10 nm.

Black Silicon is a submicrometer scale structured silicon surface obtained by surface-modification of a silicon wafer. The surface has a needle-shaped microtexture and the needles have a very high aspect ratio (typically 10) [28,29]; the depths of the holes are about 5 μm. Due to its structure, it

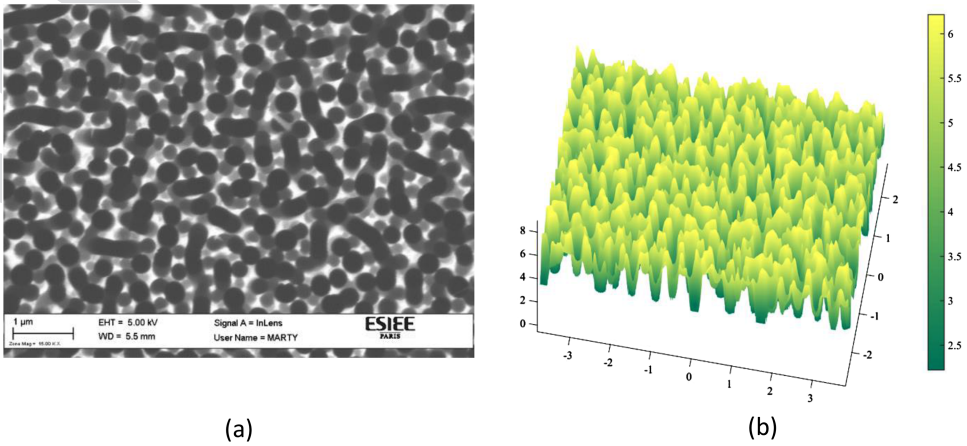

FIG. 2. (a) Top-view SEM image of Black Silicon and (b) 3D reconstruction; the unit of the scale bar is μm.

appears Black to the naked eye and has interesting wetting properties, as it can be made either superhydrophilic or superhydrophobic by subsequent thin film coatings. For instance, Teflon coating of Black Silicon makes it superhydrophobic, while silicon dioxide coating makes it superhydrophilic [30]. While different techniques can be implemented to produce Black Silicon, our samples were produced by plasma etching at cryogenic temperatures [29]. Silicon wafers were exposed to a plasma compound of SF_6 and O_2 at -120 °C under a flow rate of 200 sccm of SF_6 and 10 sccm of O_2, a pressure of 1.5 Pa, and a radio-frequency source power of 1000 W with bias voltage of -10 V. The etching time was varied from 5 to 15 min so as to reach different needle depths and related aspect ratios. Optionally, the resulting structured Black Silicon surface was subsequently conformally coated with a Teflonlike layer produced following the process described in the previous paragraph. From a top-view scanning electron microscope [Fig. 2(a)], it is possible to reconstruct the 3D topology of Black Silicon [Fig. 2(b)] by a conversion of grey level to height [31]. Figure 2 corresponds to a total etching time of 10 min. When we increase the time to 30 min, we see no noticeable change in the mean height of the needles. Teflon-coated Black Silicon is known to be a superhydrophobic surface for pure water, exhibiting large contact angles (also known as the Lotus effect) [32,33]. However, we observed that the interstitial liquid of our emulsions has a very small contact angle on Black Silicon (<5°), possibly because the liquid (water with surfactants or water + glycerol with surfactant) wets all the space between the needles, thus, the surface appears to be hydrophilic with respect to the interstitial liquid (water and glycerol mixture) of the direct emulsions.

Finally, these Black silicon surfaces provide an intermediate roughness, i.e., of the order of the droplet size. Besides, we used what we will call in the following "rough surfaces," either provided by the manufacturer (Malvern Kinexus, stainless steel, roughness = 600 μm) or made by sticking a medium grit emery cloth (OTG®, roughness ≈200 μm) on the shearing surfaces. These roughnesses are much larger than the element size, and *a priori* no slip is expected to occur in that case.

For all the three surfaces (silicon/silica, silicon with Teflonlike coating, and Black Silicon), we have measured the equilibrium contact angle of a droplet of the dispersed phase lying on the solid surface and surrounded by the continuous phase. The data are reported in the Appendix.

For MRI measurements, we used the capillary and Couette geometries. Different glass capillary diameters were used: 2, 1.2, 1, 0.8, and 0.6 mm. As for the Couette cell, the inner cylinder (diameter 16 mm) is made of PMMA, and the cup (diameter 17.95 mm) is made of glass. The gap is finally 0.975 mm. Although it is likely that the roughness of these surfaces is situated much below 1 μm, we have no more precise information.

C. Rheometry

For the rheometrical tests, we used a stress controlled *Malvern Kinexus pro+* rheometer equipped with parallel disk geometries of radius R. Except when mentioned, the disk diameter was 50 mm. The working gap (h) was 1 mm. The top plate was a serrated surface. Different surfaces are used as bottom plate: first, a serrated surface with the same roughness as the top surface and then, silicon wafers or Black Silicon surface to look at the slip behavior. The experimental procedure is as follows. We set up the sample on the bottom surface and approach the upper plate until the fixed gap is reached. Then, we remove the excess of material at the periphery. Then, we cover the sample in a water-saturated environment and start the tests. Note that the rheometer is able to impose simultaneously a vertical force and a torque to the rotating axis.

The rheometer applies a torque M to the upper plate and measures its rotation velocity Ω. The rotation of the rough upper plate implies that the velocity of the material along the upper plate and at a distance r from the axis is equal to Ωr so that the apparent shear rate in the material at a distance r is $\dot{\gamma}_0 = \Omega r/h$. Thus, the shear rate and, as a consequence, the shear stress vary with the distance from the axis. In this context, the usual approach involves computing a "mean" stress by dividing the torque by $2\pi R^3/3$. The resulting shear stress is also that which would be obtained if the stress was homogeneous in the gap since in that case: $M = \int_0^R 2\pi r^2 \tau_0 dr = 2\pi R^3 \tau_0/3$. The corresponding "mean" shear rate is taken as that observed at the distance $0.75R$ from the axis: $\dot{\gamma} = 3\Omega R/4h$. In fact, mean values do not mean anything in the absence of knowledge of the effective rheological behavior of the material and the resulting stress field in the gap. So it is more appropriate to call these variables the apparent shear stress and the apparent shear rate and write them as, respectively, τ and $\dot{\gamma}$. It is, nevertheless, worth noting that for a Newtonian behavior, the exact stress at a radial distance $0.75R$ is $3\tau_R/4 = 3M/2\pi R^2$. This means that the apparent shear rate and shear stress correspond to the exact values for the local shear stress and shear rate at this distance, and thus reflects the exact rheological behavior of the material. Furthermore, for a yield stress fluid, it may be shown that this approach provides an excellent approximation of the relationship between the shear stress and the shear rate (see the Supplementary Material of [24]).

To obtain the flow curves, we apply a sequence of creep tests, in which we impose a constant stress τ while recording the shear strain as a function of time. When the steady state flow is reached, i.e., the strain increases linearly as a function of time in log–log scale (see Fig. 4), we calculate the shear rate $\dot{\gamma}$ as the slope of the strain–time curve in the linear scale. After 5 s of rest, we repeat the same sequence for another level of τ, until obtaining the flow curve. During this sequence, we also check the reproducibility of the data at some stress values, in order to be sure that there is no significant irreversible evolution of some material characteristics or sample shape.

D. Inclined plane tests

The inclined plane is prepared by mounting the wafer on a rotary stage, by which we can control the angle of inclination i with a precision down to 0.5°. We place a sample volume,

controlled with a graduated syringe, just below the top of the wafer. Different volumes were used between 0.2 and 2 ml. For each volume, we carried out tests for different i from the lowest to the largest possible values (depending on the material behavior). When placed on the solid surface, the sample may slightly spread and move along the steepest slope.

To record the form and the displacement of the drop, a camera was placed above the wafer. We started recording immediately after loading the sample. The sampling frequency ranged between 0.125 and 1 frames per second. To quantify the displacement and the contact area of the sample with the solid surface, we covered a part of the wafer with a graph paper. We used ImageJ to calculate and plot the instantaneous position (with respect to the initial position) as a function of time. To do so, we set the scale of the image using the graph paper in the recorded images to convert pixels into SI units, then we fitted the image of the sample with a polygon to calculate the contact surface S. After binarizing the images, we used Multitracker plugin in ImageJ to obtain the position of the centroid of the image as a function of time.

E. MRI velocimetry

MRI Velocimetry in capillaries has been performed in LEMTA at Université de Lorraine. A flow rate-controlled syringe injects the inverse emulsion (72 vol. %) to the capillary positioned inside the magnet at different flow rates. Longitudinal velocity measurements start once a stationary flow is established. The velocity profile acquisition was carried out with Bruker Avance III 600 Wide Bore spectrometer (magnetic field B = 14.1 T, 600 MHz proton resonance frequency) with 150 G/cm gradient system. The microimaging probe (MicWB40) used is manufactured by Bruker and it is equipped with a 10-mm-diameter resonator. The velocity profiles are acquired using a flow encoding spin-echo protocol: classical spin-echo MRI experiment with in addition bipolar gradient pulses in order to encode the phase shift arising from the flow [34]. The geometrical parameters are as follows: the field of view (FOV) is 0.3 cm × 0.3 cm (for the capillaries of 2 and 1 mm diameter) and 0.4 cm × 0.4 cm (for the capillaries of 1.2, 0.8, and 0.6 mm diameter); the thickness slide ranges from 0.2 to 1.5 cm and the matrix is 256 × 256 pixels. The acquisition time is about 1 min. The velocity profiles (pixel size) obtained have a spatial resolution of about 10 μm (for the capillaries of 2 and 1 mm diameter) and 16 μm (for the capillaries of 1.2, 0.8, and 0.6 mm diameter). For each 2D flow map, we represent the velocity in each pixel as a function of its distance to the center, then average to finally obtain a single velocity profile for each flow rate.

MRI velocimetry measurements in the Couette cell have been carried out in Bruker Biospin GmbH. The NMR method for the velocity measurement is a "Pulsed Gradient Spin Echo Velocity Imaging" sequence [35], generating 2D spatially resolved velocity maps from which 1D velocity profiles across the gap of the Couette cell are extracted. The Couette cell characteristics are the following: the inner cylinder, made of PMMA, has a diameter of 16 mm and a length of 99 mm, and the outer cell, made of glass, has a diameter of 17.95 mm and a length of 103 mm. The inner cylinder is mounted to a motor, capable of controlling the rotation velocity from 0 to 10 Hz (0.5 m/s on the surface of the inner cylinder). The outer cup is kept static. The Couette cell is immerged into a static field of 300 MHz (7 T). The temperature is fixed at 25 °C. In the plane perpendicular to the axis of the cylinder, the acquisition window is a parallelogram of radial length 6.4 mm, tangential width 10 mm, and thickness (along cylinder axis direction) 12 mm. We then obtained a 2D velocity map in a plane perpendicular to the cylinder axis, from which we extract the velocity profile along a radius by averaging data over a (tangential) thickness of 1.25 mm. To determine the slip velocity along the inner cylinder surface, we fit the profiles near the wall with a linear function and the velocity associated with its intersection with the wall is then subtracted from the imposed tangential velocity of the cylinder. The slip velocity at the outer cup wall is directly obtained from the intersection of a linear function fitted to the profile near the wall. The validity of this (basic) approach was confirmed by checking that it gives a negligible wall slip velocity from measurements with a Newtonian fluid (water + glycerol).

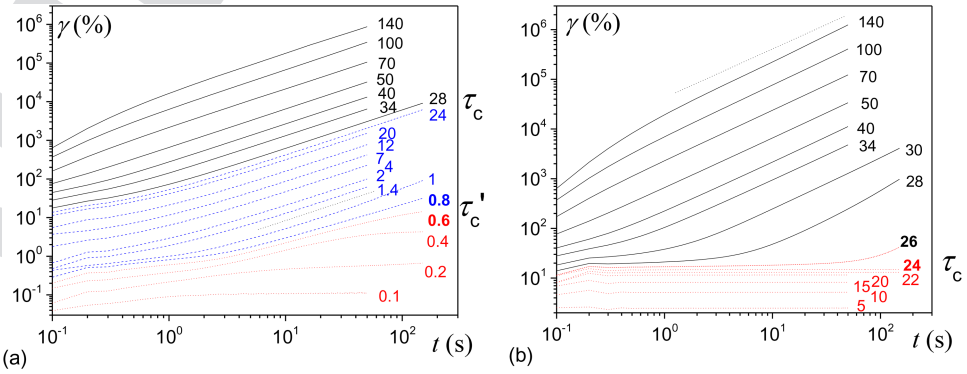

FIG. 3. Typical aspect of creep tests for a yield stress fluid (emulsion A1) and different solid surfaces: shear deformation as a function of time. (a) Smooth bottom surface; red dotted curves correspond to the solid regime, blue dashed curves to the slip regime, and black curves are the shear regime; in this example, the slip yield stress τ_c' is situated between 0.6 and 0.8 Pa; (b) rough surfaces; red dotted curves indicate the solid regime, black curves indicate the shear regime; here the yield stress τ_c is situated between 26 and 28 Pa, even if there is some residual deformation at long times at 26 Pa, it does not seem to reach a steady state flow (with a slope 1 in the logarithmic scale). The stress levels in Pascals are indicated in the figures. The short straight dotted lines in both figures with a slope 1 serve as a guide for the eye; a linear evolution of the deformation with time corresponds to a steady simple shear.

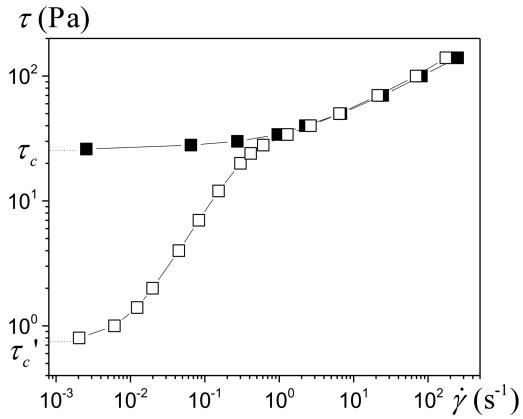

FIG. 4. Flow curves deduced from the steady state flow data of Fig. 3: bottom smooth surface (open squares) and rough surfaces (filled squares).

III. EXPERIMENTAL RESULTS

A. First results

Let us first look at the material behavior during creep tests with a smooth surface [Fig. 3(a)]. For stress below a critical yield stress τ_c', also called the slip yield stress, the material undergoes a small deformation, typically below a few percents, which finally reaches a plateau, indicating that there is no more motion; the material's response in that case is that of a solid. For stress larger than τ_c', the deformation is larger and finally, increases linearly with time, indicating that a steady state flow is reached (apparent liquid regime). A critical point in this approach is that we determine the slip yield stress, not by fitting some function in the slip regime, but by determining its exact value from the observation of the transition between two regimes (i.e., flow or stoppage).

Creep tests with rough surfaces, i.e., for which we *a priori* do not have wall slip, yield similar results but the transition between the apparent solid and liquid regimes occurs at a higher level [see Fig. 3(b)], which now corresponds to the yield stress τ_c, the stress for which the bulk starts to flow in its liquid regime. Beyond this yield stress, the material behaves as a simple yield stress fluid, with no significant time effects: the flow curve is the same whatever the procedure (after different times of rest or by starting from high shear rates). From these results, we deduce that between τ_c' and τ_c, the bulk is in its solid regime so that it only undergoes limited deformations which cannot be at the origin of the steady state flow observed with smooth surfaces. As a consequence, in this regime, the bulk material moves as a rigid block along the solid surface of the tool. Moreover, there necessarily exists, between the bulk and the solid surface of the tool, some layer of a material of different nature (e.g., the interstitial liquid, possibly with some suspended elements) which is sheared between the bulk and the wall. Thus, we may compute the slip velocity, i.e., the relative velocity between the bulk and the smooth wall, from the apparent shear rate, $V_s = \dot{\gamma} h$.

The slopes of the deformation vs time curves in the steady state flow regime may be used to plot the apparent flow curves, with or without rough surfaces (see Fig. 4). Note that here both τ_c and τ_c' are precisely defined, i.e., we are sure that no steady state flow or wall slip can be obtained for a stress below τ_c'. This makes it possible to distinguish clearly the slip regime below the yield stress and then deduce the slip velocity. Note that around the yield stress the two curves (with smooth or rough surfaces) flatten and tend to superimpose. In that case, there may still exist some wall slip for smooth surfaces, but since now the apparent velocity results from both a bulk flow and a wall slip the above straightforward reasoning, allowing to deduce the wall slip velocity is not sufficient. An approach would involve withdrawing, for each stress value, the shear rate observed with rough surface from the apparent shear rate with smooth surfaces, to get the apparent shear rate resulting from wall slip. However, this procedure can hardly provide reliable data due to the high sensitivity of shear rate to stress for the bulk flow and the sensitivity of the stress to the exact shape of the sample at its periphery [2]. A measure of the possible wall slip when a bulk flow exists should be carried out with a technique allowing a direct internal measurement.

Although the qualitative trends of creep tests for all materials are similar, a distinction appears between direct and inverse emulsions concerning the characteristics of their flow curve. For direct emulsions, τ_c' may slightly fluctuate if we repeat the test. For inverse emulsions, τ_c' appears to be significantly larger than the values observed with direct emulsions and varies in a wider range. This point will be discussed further in Sec. III B.

B. Origin of the wall slip yield stress

1. Direct emulsions

In inclined plane tests, we observe that while the drop of (direct) emulsion slowly moves downward, two lines of deposit of material remain along the sides of the drop [23]. We also note that a very thin liquid layer may appear on the solid surface at the rear of the sample, but quickly evaporates, and then we do not detect any more liquid on the solid surface in this region. It can be concluded that the material slips along most of its surface of contact with the plane, but some bulk material may be sheared along the edge of the sample.

Let us now examine the consequences of this effect on rheometrical tests. To start with, we check that it also occurs in a rotational geometry. Instead of a full circular layer as for standard rheometrical tests, we confine a smaller volume (i.e., a drop) of material between the two disks of the rheometer, with the drop center placed at some distance from the axis. Under these conditions, when the upper (rough) disk rotates, it drifts the material in rotation around the axis and the squeezed drop slips over the smooth bottom surface. Then, we observe that there remains a circular track of bulk material around the internal and external edges of the sample [see Fig. 5(a)]. These tracks are typically a few hundreds micrometers to 1 mm thick and wide. From this observation, we deduce that there is such a small volume of material sheared at the periphery during a standard rheometrical test, i.e., with the sample filling all the gap between the tools, but it is not directly visible since the material always covers the whole surface of contact.

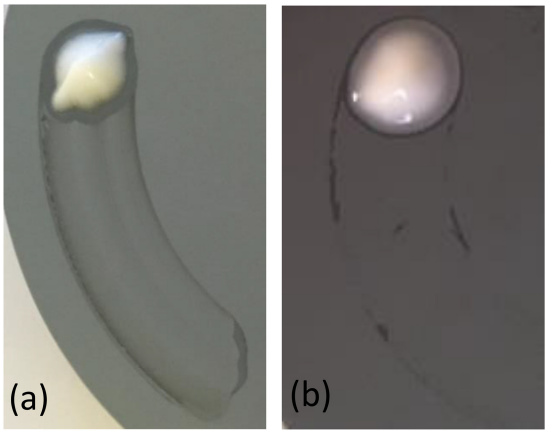

FIG. 5. Aspect of a drop of material drifted by the top plate of the rheometer, after separation of the plates and a circular motion: (a) direct emulsion (width 1.6 cm) and (b) inverse emulsion (width 1.35 cm).

It was suggested [23] that this edge effect is at the origin of the residual yield stress with smooth surfaces. Indeed, if wall slip is associated with the flow of a liquid in some given geometry, it is expected to occur and thus allow some flow under any stress value. In contrast, if some region (here along the periphery) of the material is sheared, a stress larger than the yield stress is required in this region, which on average will induce an apparent yielding behavior, even if the rest of the material slips along the solid surface.

More precisely, let us assume that the slip conditions along most of the surface of contact with the bottom plate require to apply a torque M_0, related to the apparent shear stress $\tau_0 = 3M_0/2\pi R^2$. Then we assume that some edge effect induces a stress (τ_c) acting over a constant width (e) along the sample periphery. This situation would, for example, be encountered if a layer of (radial) width e was stuck to the smooth plate and induced a shear of the surrounding material at the approach of this zone. This effect will induce an additional torque, $2\pi R^2 e\tau_c$ so that the total torque becomes $M_0 + 2\pi R^2 e\tau_c$, and the apparent stress has now an additional component: $\tau \approx \tau_0 + 3e\tau_c/R$. Note that this approach is a rough description of reality as we ignore the exact shape of the sheared region, its possible variation with velocity, and the slight increase of the stress from τ_c as the local shear rate increases.

From this analysis, it is obviously expected that such an edge effect plays a minor role when the sample surface to the perimeter ratio is sufficiently large, e/R, when is sufficiently small. A series of tests with different sample radii effectively show that, for a given material (with a constant yield stress), τ_c' increases when the sample radius decreases [see Fig. 6(a)]. If we consider, for example, the data for a disk radius of 6 cm, τ_c' is typically of the order of 1 Pa, which means that e should be of the order of 250 μm. This is in the same order of magnitude of the width of the tracks left behind the displacement of a drop, which is around 0.5 mm [see Fig. 5(a)]. It is not possible to elaborate further on that point as this would require knowing the exact shape of the arrested layer at the periphery.

The origin of this effect might be that some suspended elements tend to be attached to the solid surface at the contact line, as a result of a slight evaporation effect at the contact line, more or less as in the coffee-ring effect [36]. Here, we further examine the validity of this statement by observing the impact of the time of rest before applying a stress, since it is expected that an effect associated with evaporation should be larger for longer times of drying.

We performed tests under controlled shear rate with smooth surfaces as follows: after setting up the sample in the geometry, we did not surround it with a vapor saturated environment so that it could more rapidly dry; we thus left it at rest for a given time, imposed a low shear rate (0.01 s^{-1}), and recorded the shear stress evolution (see Fig. 7) for some time; then, we cleaned the geometry and set up a new sample for a similar test with a different time of rest. The stress vs time curves look like those obtained for creep tests with yield

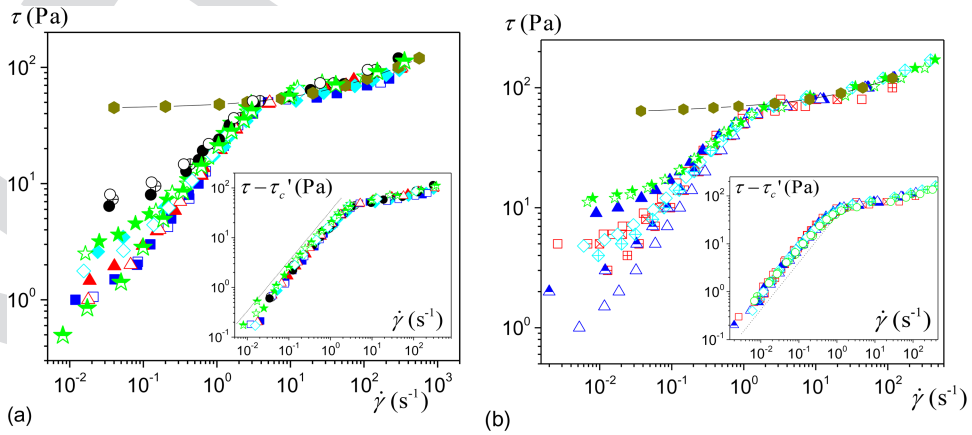

FIG. 6. Apparent flow curves on smooth surface of (a) a direct emulsion (82%) (data from [24]) and (b) an inverse emulsion (82%) for the same gap and different plate diameters: 9 cm (squares), 6 cm (triangles), 4 cm (diamonds), 3 cm (stars), 3 cm with oil film at the sample periphery (half-filled stars), and 2 cm (circles). Hexagons show data with two rough plate surfaces. Several tests were carried out by changing the sample while keeping the same surface are shown for each diameter in order to appreciate the reproducibility of these experiments. Open triangles correspond to test after lens paper cleaning, while the other data correspond to acetone + compressed air cleaning. Note that in order to remove the impact of sample shape at the periphery, which increases when the sample radius decreases, τ has been rescaled by a factor around 1 to get the same stress values at the yielding transition (see [24]). The insets show the stress minus the wall slip yield stress vs shear rate for the same data. The dotted lines of slope 1 are guides for the eye.

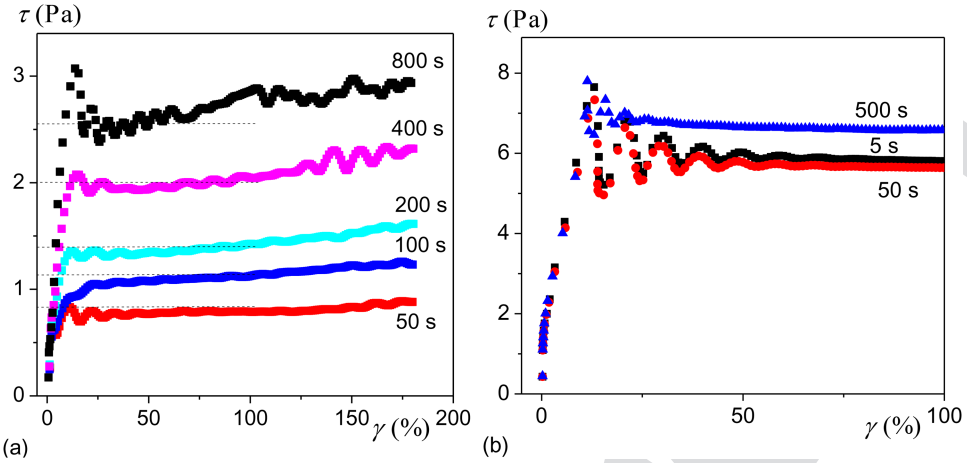

FIG. 7. Shear stress as a function of shear strain while imposing a shear rate $\dot{\gamma} = 0.01\ s^{-1}$ to (a) a direct emulsion B and (b) an inverse emulsion (82%) after different times of rest (indicated in the graph close to the corresponding curves) prior to the experiment on a smooth surface; the dashed lines indicate the assumed level of τ_c'.

stress fluids [2]: after an increase the stress reaches a plateau; note, however, that there are some oscillations at the beginning, which likely result from the fact that the stress controlled rheometer imposes a constant low shear rate with the help of a feedback loop. Since the imposed shear rate value is around the critical shear rate value below which flow stops with smooth walls in our other tests (see Figs. 3 and 4), we can consider that the stress plateau level (taken in the initial horizontal part, before the slight increase) here observed would correspond to the wall slip yield stress. Under these conditions, it is remarkable that this slip yield stress increases significantly with the time of rest [see Fig. 7(a)], approximately with the square root of the time of rest. A second remarkable observation is that the increase of the stress during the flow is smaller than that resulting from the rest over a similar duration [this may be seen from the curves for the smallest times of rest (smaller than the creep test duration, i.e., 180 s)]. This means that the wall slip yield stress essentially evolves when the material is at rest, and only slightly evolves over the typical time of flow of creep tests. This proves the validity of our series of creep tests for consistently determining the behavior of the materials below the yield stress: we impose successively increasing stress levels; the material starts to flow for some critical stress associated with the flow history from the beginning; since (i) the next tests are carried out at larger stress values, they also induce a flow, during which the wall slip yield stress does not increase much, and (ii) the tests are carried in a vapor saturated air, which considerably limits the drying so that the wall slip yield stress even increases less during our series of creep tests and, finally, can be considered as constant.

From the above analysis, we conclude that withdrawing τ_c' from the stress should reveal the shear stress solely associated with the wall slip along the area of contact between the sample and the solid surface. And indeed, we observe an excellent superimposition of the curves of $\tau - \tau_c'$ vs $\dot{\gamma}$ for the different sample diameters [see inset of Fig. 6(a)], showing that removing the edge effects give a unique wall slip flow curve. We call the stress strictly associated with wall slip, τ_S, and define it as $\tau_S = \tau - \tau_c'$. Then V_S as a function of τ_S can be considered as the wall slip law of the material over a given surface. It appears that for the tested emulsion this law is linear [see inset of Fig. 6(a)], i.e., $\tau - \tau_c'$ is simply proportional to $\dot{\gamma}$, and thus to the slip velocity $V_S = h\dot{\gamma}$. We deduce that we can write $\tau_S = \alpha V_S$, and expressing α as $\alpha = \mu/\delta$, where μ is the viscosity of the interstitial liquid and δ a characteristic length, we get

$$\tau_S = \mu V_S/\delta. \quad (1)$$

Under these conditions, δ has a physical meaning: if we assume that the slip occurs as a result of the simple shear of a uniform layer of (pure) interstitial liquid along the wall while the bulk remains rigid, δ is the thickness of this layer. Moreover, from Eq. (1), we deduce the slip law expressed as a relationship between dimensionless parameters:

$$\tau_S/\tau_c = (1/\delta)(\mu V_S/\tau_c), \quad (2)$$

which, in particular, allows one to proceed to a relevant comparison of results obtained with materials with different interstitial liquid viscosities.

2. *Inverse emulsions*

This origin of the wall slip yield stress, i.e., an edge effect due to the adherence of the material around the line of contact as a result of evaporation, can hardly apply to inverse emulsions. Indeed, the water droplets are covered with an oil layer, which considerably slows down evaporation, and even if they finally evaporate, this will increase the local concentration of oil, which should *a priori* foster wall slip. Actually, we effectively do not see lateral tracks of the bulk material when a drop is moved over the smooth surface [see Fig. 5(b)]: the dark areas appearing in the photo along the edges of the drop trajectory have apparently the same thickness as the extremely thin oil layer covering the rest of the surface and left behind the drop. Moreover, we observe that there is no significant impact of the time of rest on the value of τ_c' for inverse emulsions [see Fig. 7(b)], in strong contrast

with direct emulsions [see Fig. 7(a)]. These observations confirm that for inverse emulsions, the main origin of the wall slip yield stress is not an edge effect.

Two other aspects distinguish the wall slip yield stress for inverse emulsions: τ_c' is larger for direct emulsions, and its value fluctuates widely, as appears from reproducibility tests [see Fig. 6(b)]. Although we can suspect that the origin of this effect is the exact history of the surface cleaning before each test, we were unable to distinguish a clear trend, except one point: the standard procedure involves cleaning the surface with acetone, then blowing it with compressed air; smaller τ_c' values were generally obtained when before set up the solid surface is rubbed with a lens paper. Finally, it does not seem possible to distinguish an increase of τ_c' with the decrease of the sample diameter, the flow curves in the slip regime are scattered in the range of variations obtained for a single diameter [see Fig. 6(b)], without specific trend. This confirms that for inverse emulsions, the wall slip yield stress does not find its origin in an edge effect. As a consequence, this is an effect which takes place along all the surface of contact between the material and the solid surface, typically some slight interaction between the droplets and the solid surface.

This interaction apparently takes the form of an adhesion force, whose level is very sensitive to the exact preparation of the surface, which implies that we have to present the results as a set of flow curves illustrating the range of variation of τ_c'. If we now withdraw the value for τ_c' obtained in each of these tests, so as to represent $\tau - \tau_c'$ vs $\dot{\gamma}$, we again find that all the data fall along a single master curve [see the inset of Fig. 6(b)]. This means that, for inverse emulsions, the wall slip law (in terms of shear stress) is the sum of a friction term, very sensitive to exact conditions, plus a constant function of the shear rate.

3. Conclusion concerning the origin of the wall slip yield stress

The above observations for two types of emulsions provide two different situations leading to an apparent wall slip yield stress.

1. An edge effect: some material is stuck along the peripheral line of contact, which induces a shear along a small surface at the periphery, leading to an apparent yield stress at low velocity; the characteristics of this effect are: a thin bulk deposit along the lateral edges of a drop displaced along the solid surface, an increase of this effect with the time of rest, and an increase of this (edge) effect for decreasing sample radius. In addition, the order of magnitude of this effect may be estimated from the above rough approach: the sheared surface is typically of the order of 200 μm (as deduced from our observations with emulsions), during current tests (with no times of rest exceeding 100 s), which induces a ratio τ'_c/τ_c of the order of $3e/R \approx 0.6/R$ (with R in millimeters).
2. A surface effect: the elements of the material tend to adhere onto the solid surface, and some critical stress is needed to break these links; the characteristics of this effect are: no thin bulk deposit along the lateral edges of a displaced drop, no increase of this effect with the time of rest, and no impact of the sample radius. For the inverse emulsion, it also appears that the value of the wall slip yield stress widely fluctuates, which will in fact appear as a general characteristics of surface effects in the following.

Note that these two types of behaviors, i.e., negligible and significant (with regard to τ_c) wall slip yield stresses, were already observed with emulsions, respectively, over a well-controlled non-adhering and a weakly adhering surface [37]. However, in the latter case, a quadratic variation of the slip velocity with $\tau - \tau_c'$ was observed, in contradiction with our results.

Determining whether we are dealing with an effect of type 1 or 2 is not so easy in practice. The conclusion can be immediate if one observes a ratio τ'_c/τ_c significantly larger than $0.6/R$, since then it is unlikely that edge effects could induce such a high stress. When this is not the case, i.e., the two values are of the same order of magnitude, the diagnosis requires a full enquiry, such as the tests described above. It may also happen that both effects play a role, an even more

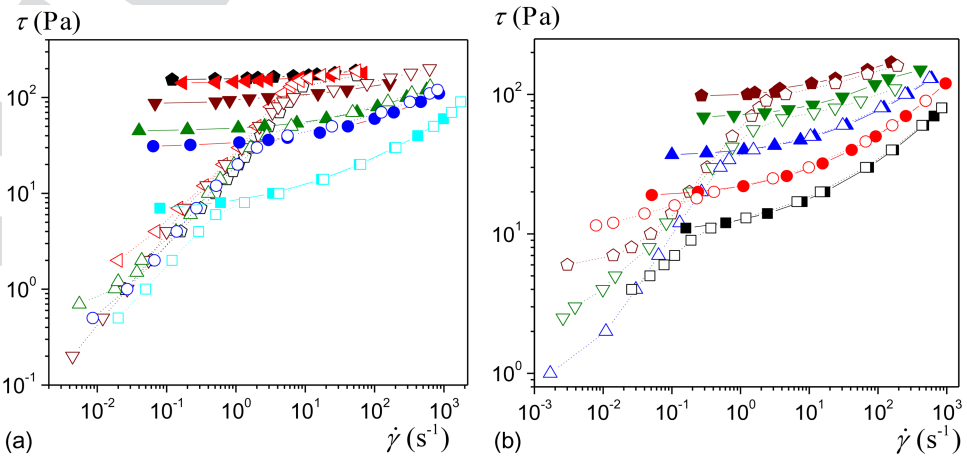

FIG. 8. Flow curves, as deduced from steady state flows in creep tests, for (a) direct emulsions (composition B) at increasing concentrations: (from bottom to top): 72%, 78%, 82%, 86%, 90%, 92% and (b) inverse emulsions at increasing concentrations: (from bottom to top) 72%, 74%, 78%, 82%, 86%. Open symbols correspond to smooth bottom surface, filled symbols to rough surfaces.

complex situation, for which it might be ultimately extremely difficult to conclude.

C. Impact of concentration

The flow curves, deduced from steady states in creep tests, for the direct emulsion at different concentrations and for smooth or rough surfaces are shown in Fig. 8(a). As expected, the yield stress increases with the concentration but, remarkably, the flow curves in the presence of wall slip below the yield stress appear to essentially follow a master curve independent of the concentration, except at the approach of τ_c', which takes different values below 1 Pa. Note that the data for the 72% emulsion correspond to a slightly higher slip velocity. We do not have an explanation for that trend, this may be either due to the fact that the concentration is close to the critical concentration beyond which jamming occurs and a true yield stress is clearly observed (around 70%) or to the uncertainty on data, or both.

This means that both the slip yield stress and the wall slip law are independent of the concentration. Thus, the part of flow curve with wall slip of an emulsion at some concentration may be directly deduced from a measure of wall slip at another concentration. As expected from the flow curves, it appears that, for the direct emulsions, the wall slip laws at different concentrations fall along a single master curve (see Fig. 9), indicating that, if concentration has some effect, it is weaker than the uncertainty on measurements. This master curve is linear, which means that the slip velocity is proportional to the slip stress.

For the inverse emulsions, it is more difficult to appreciate the impact of concentration on the wall slip flow curve, due to the large scattering on the slip yield stress [see Fig. 8(b)]. However, the slip yield stress remains in the same (wide) range observed for a series of tests at the same concentration [see Fig. 6(b)], a range once again typically 1 order of magnitude larger than that observed for τ_c' for direct emulsions at different concentrations [see Fig. 8(a)]. Moreover, after withdrawing τ_c', the shear stress appears to be also proportional to the slip velocity but with an apparent thickness of the slip layer smaller than for direct emulsions (see Fig. 9). One may also note that the data tend to depart from the line of slope 1 in logarithmic scale for large stress values, indicating a faster increase of the slip velocity as a function of the stress.

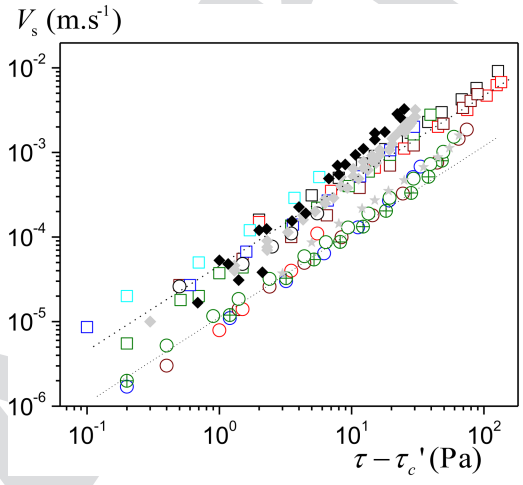

FIG. 9. Slip velocity (over smooth surface) as a function of the slip stress for direct emulsions at the different concentrations presented in Fig. 8(a) (squares, same colors) and for inverse emulsions at the different concentrations presented in Fig. 8(b) (circles, same colors). The upper dotted line corresponds to the function $\tau_s = \mu V_s/\delta$, with $\mu = 0.89$ mPa s and $\delta = 35$ nm, and the lower dotted line to the same function with $\mu = 1.36$ mPa s and $\delta = 15$ nm. Data for Teflonlike surface (filled grey symbols) and Black Silicon surface (black filled symbols) are also presented for the direct (diamonds) and the inverse emulsion (stars).

D. Impact of surface characteristics

The detailed impact of surface roughness or surface interaction between the fluid and the solid has been studied through detailed measurements of the flow characteristics at a local scale, by few authors [38–40], in the yielding regime. These works were carried out essentially in the frame of confined flows, i.e., with characteristics flow length (typically, the gap between the two solid boundaries) not very much larger than the element size. It was, in particular, found that in this context, the roughness or the hydrophobicity may alter wall slip properties. It was also shown from internal velocity measurements that the surface–fluid interaction has a long range action, leading to some unexpected shear at some distance from the wall [37]. These different results were interpreted within the frame of the fluidity model.

Here, we focus on the impact of surface characteristics on wall slip under conditions for much larger gap sizes so that possible confinement effects *a priori* have a negligible influence, and we focus on the slip regime below the yield stress. In that aim, we first look at the behavior of direct emulsions in contact with Black Silicon surfaces, which have an apparent roughness of the order of the droplet size (see Sec. II A). Such a roughness can thus be considered as intermediate between the smooth silicon surfaces and the rough (serrated) surfaces. From creep tests at different stress levels (see Fig. 10), we see that the material reaches a steady flow for a stress larger than the yield stress, but can also reach a steady flow between a lower stress (τ_c') and the yield stress. It does

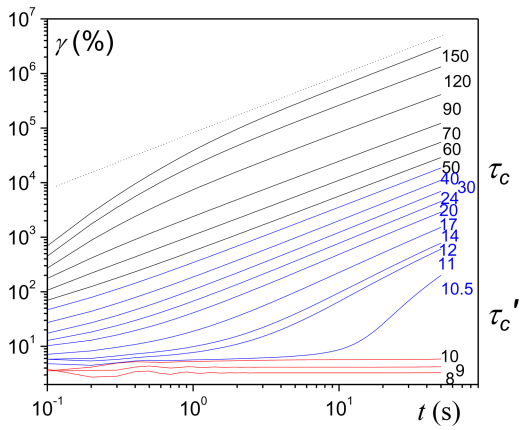

FIG. 10. Creep tests for emulsion B on Black Silicon surface (shear stress values applied are mentioned in Pascals); red curves correspond to the solid regime, blue curves to the slip regime, and black curves to the liquid regime; the slip yield stress τ_c' is situated between 10 and 10.5 Pa. The sample diameter here is 5 cm.

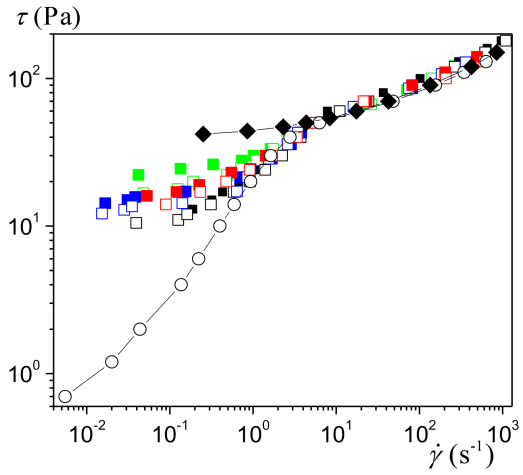

FIG. 11. Flow curve deduced from creep tests for emulsion B (82%) with rough (serrated) surfaces (diamonds), bottom smooth surface (open circles), and bottom Black Silicon (squares) with different sample diameters: (green) 3 cm; (black) 5 cm; (blue) 6 cm; and (red) 9 cm. Empty/filled symbols distinguish two different tests under the same conditions.

not flow for a stress below τ_c'. This means that the roughness is not sufficient to avoid any type of wall slip, and some wall slip effect can develop, which leads to an apparent flow curve situated between the flow curve of the material and the wall slip flow curve over a smooth surface (see Fig. 11).

The apparent wall slip obtained with the Black Silicon surface has some specific characteristics. First of all, we notice that, in creep tests, the transition between the solid state and the wall slip is rather abrupt (see Fig. 10), precluding any steady state flow at an apparent shear rate lower than $10^{-1}\ s^{-1}$. Moreover, here, considering the large value of τ_c', the wall slip yield stress is undoubtedly due to a surface effect. This is confirmed by the tests at different diameters (see Fig. 11), τ_c' varies in the range 10 to 20 Pa, but there is no clear correlation between its value and the sample diameter. It is likely that the micro roughness of this surface tends to block, at least provisionally, some droplets, as in a small potential well so that some minimum stress is needed to move out the droplet from this potential well and allow for a steady state motion. Note that there might remain some edge effects as for smooth surface, but its level is much lower than the apparent value for τ_c' so that it does not induce significant variation of τ_c' (it might, nevertheless, become significant for a small diameter, which could explain the apparent larger τ_c' value for 3 cm diameter in Fig. 11). Finally, it is interesting to compare the relationship between the additional wall slip stress (i.e., $\tau_s = \tau - \tau_c'$) and the slip velocity with the same relationship for smooth surface. It appears that the slip velocity with the Black Silicon surface is similar for that for smooth surface for low stress but tends to be significantly larger (see Fig. 9), by a factor about 2, for larger stress.

With Teflonlike surface, the flow curve of direct emulsions now also exhibit a fluctuating τ_c', but anyway much larger than that observed over silicon surface [see Fig. 12(a)]. This situation is similar to that observed for inverse emulsions over silicon surface, which suggests a similar physical origin, i.e., some kind of (provisional) adhesion of the droplets onto the solid surface. The impact of Teflonlike surface on the wall behavior of inverse emulsions is stronger. Now, wall slip may completely disappear [see Fig. 12(b)]: a 74% emulsion flows without wall slip with rough or Teflonlike surface.

These observations suggest that, for a given material, a solid surface induces a given adhesion effect associated with some particular stress value, which may be smaller or larger than the material yield stress. In the former case, wall slip will occur, in the latter case, wall slip will not occur since the minimal stress needed to induce wall slip is larger than the yield stress and thus induces bulk flow. This is confirmed by further tests with a very concentrated inverse emulsion, with a yield stress much larger than the 74% emulsion [see Fig. 12(b)]: with the same Teflonlike surface, we now have a wall slip regime, with a τ_c' value smaller than the yield stress but larger than the yield stress of the 74% emulsion for which no wall slip was observed with Teflonlike surface.

Let us finally mention that we also tested PMMA and glass surfaces on bottom plates, for direct and inverse emulsions, but the results did not offer sufficiently significant

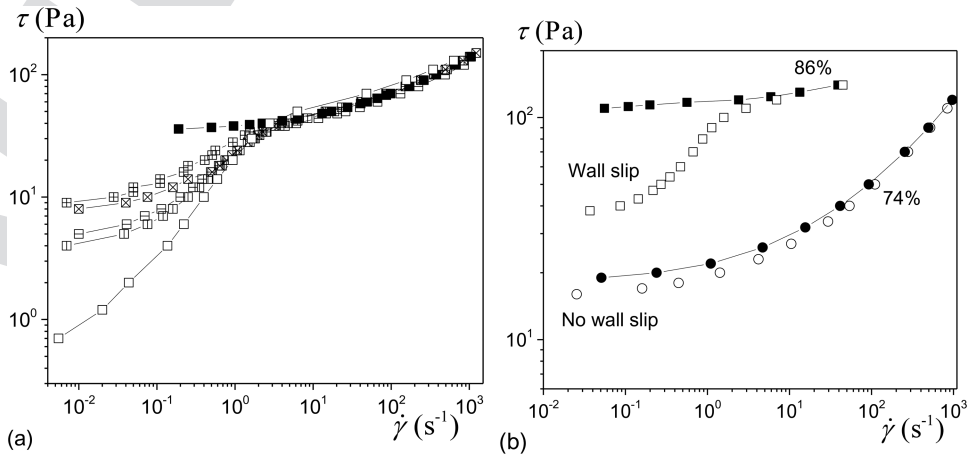

FIG. 12. Flow curves, as deduced from steady state flows in creep tests, for (a) emulsion B (82%) with rough surfaces (filled squares), smooth surface (open squares) or Teflonlike surface (cross-squares), and for (b) 74% (circles) and 86% (squares) inverse emulsion with rough surfaces (filled symbols) or Teflonlike surface (open symbols).

differences with those observed with silicon surface. In some cases, a slightly larger value for τ_c' than with silicon surface was observed, but it is not possible to definitely conclude about a possible different physical process.

E. Impact of material structure

We may look at the impact of a change of the material structure by varying the droplet size distribution of emulsions. The flow curves of direct emulsions with different droplet sizes with rough or smooth surfaces are shown in Fig. 13(a). We observe that, in addition to the increase of τ_c with $1/r$ discussed in Sec. II A, all the emulsions exhibit wall slip on the silicon wafer. However, we do not obtain a clear, unique master curve for the stress vs shear rate in the slip regime for the different droplet sizes. At first sight, there seems to be some slight increase in the slip velocity with the droplet size for a given stress. These observations are confirmed by the results represented in terms of slip velocity vs rescaled slip stress [see Fig. 13(b)]. As for the above emulsions, we find that the data follow a straight line of slope 1, but we also observe a slight tendency to departure from this line at the approach of the yield stress. Actually, this departure occurs earlier for increasing droplet size [see Fig. 13(b)]. Moreover, there seems to be a slight evolution, larger than the usual noise on such data, when the droplet size increases: the slip velocity, or equivalently the apparent slip layer thickness, fitted to data [see inset of Fig. 13(b)] increases by a factor about 2 when the (average) droplet size increases from 1.1 to 11 µm. However, this value (i.e., 2) is still relatively low with regards to the general scattering on such data so that we can hardly consider that we here evidenced a clear trend.

By the way, we see that with this rescaling, the data fall along the same master curve as the data for emulsion B of viscosity smaller by a factor about 5 [see Fig. 13(b)]. This confirms the generality of the expression for the slip law [Eq. (2)].

F. Impact of flow conditions

Previous works essentially focused on wall slip properties when the fluid is constrained between two solid tools (in a rheometer) and without particularly controlling the normal stress. Here, we intend to evaluate the wall slip properties under different flow conditions with two aims: possibly some better understanding of the physical mechanisms at work in wall slip, and test of the applicability of the slip law deduced from rheometry to different flow conditions.

1. Impact of normal stress

In order to get a further insight into the physical origin of wall slip, and in particular, to test the possibility of some balance between attractive and repulsive forces, it is interesting to test the impact of a normal force on the wall slip. According to the concepts of Princen [22], Le Merrer *et al.* [19], and Meeker *et al.* [11,16], the slip layer would be governed by a balance between repulsive and attractive forces, the latter resulting from the repulsion between the components of the material which, in a microgel suspension, an emulsion or a foam, is related to the mechanical properties of the material. There thus exists a kind of osmotic pressure, tending to push the droplets against the solid surface ("attractive force"), and which can be related to the elastic modulus of the material [41]. Now, if additional external forces also tend to push the droplets against the wall are applied, the balance of forces should be displaced, leading to a change in the slip layer thickness. We can test this effect by imposing a nonzero normal stress difference to the system (with a force applied along the sample axis). The interesting point is that such yield stress fluids are able to support some normal stress difference (below a critical value) without flowing. As a consequence, the structure is only slightly deformed but this structure is pushed against the wall with this additional force.

We carried out rheometrical tests under our standard conditions in simple shear but now imposing larger normal stresses. More precisely, we varied the normal stress in the widest range over which this stress does not induce an elongational flow of the material in its liquid regime (i.e., yielding in elongation). For a direct emulsion (82%, $\tau_c = 45$ Pa), we did not observe any significant effect (difference less than 1.5%) on the slip velocity when the normal stress was varied in the range $-200 + 200$ Pa. Note that we do not have a clear explanation of what sets this maximum stress amplitude

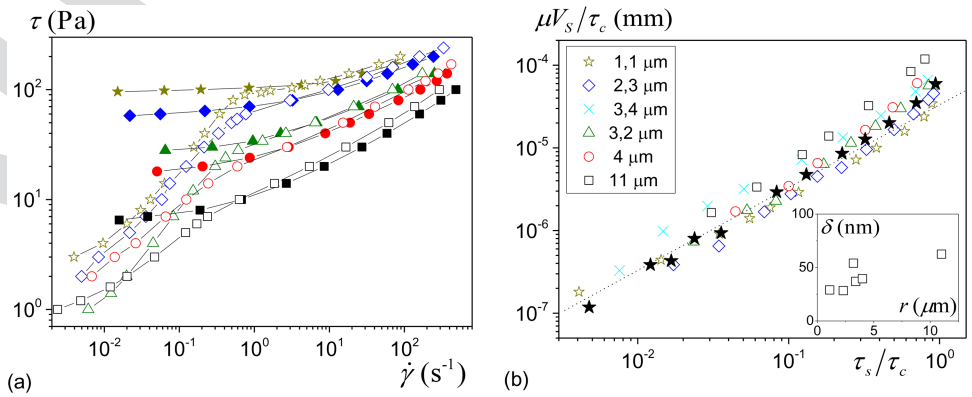

FIG. 13. (a) Flow curves for emulsions A with different mean droplet sizes (from top to bottom: A1 to A5) with rough (filled squares) or smooth bottom surface (empty squares); (b) slip velocity as a function of slip stress rescaled by the yield stress. Filled stars correspond to emulsion B (2 µm). The oil concentration of the emulsions is 82%. The inset shows the apparent slip layer thickness fitted to the data as a function of the mean droplet radius.

below which there is no elongational flow. We can just note that if the two walls were smooth, we would expect a bulk flow (elongation) in the liquid regime for a stress equal to 117 Pa (i.e., $1.5\sqrt{3}\tau_c$, according to [42]), but here the boundary conditions are more complex (smooth and rough walls). For an inverse emulsion (82%, $\tau_c = 65$ Pa), we did not either observe more significant variations than the standard scattering in data of the slip velocity when a normal stress amplitude was varied up to 300 Pa, either in the positive or the negative range.

Let us now compare the value of this additional stress to the osmotic pressure of the material. On the basis of measurements on monodisperse emulsions [41] and generalization (in particular, for polydisperse materials) [43], we can estimate the osmotic pressure to be of the order of 5000 Pa for the 82% emulsions. As a consequence, the impact of a normal stress, even close to the largest value before yielding, should be negligible compared to the osmotic pressure. Finally, within the frame of the models assuming some balance between repulsive and attractive forces (see above), it is thus not surprising that such normal forces do not affect wall slip.

2. *Wall slip in unconfined flows*

When a drop of emulsion is put on the inclined silicon wafer, it may slightly slump due to its own weight [44,45] if its volume is large enough (typically larger than 0.4 ml), whereas for smaller volumes, the drop apparently does not slump. Besides, the weight component parallel to the surface tends to move the sample downward. When this occurs, the shape reached by the drop after a possible initial slump remains constant, indicating that the bulk material is in its solid regime and slips along the solid surface. Finally, the drop advances faster for larger slopes [Fig. 14(a)] and larger volumes [Fig. 14(b)].

We can compute the mean shear stress τ acting on the sample along the solid surface according to the shear stress derived from the momentum balance:

$$\tau = \rho\Omega g \sin i/S. \tag{3}$$

From Eq. (3), the observed variations of slip velocity with volume and slope appear consistent.

When this stress becomes larger than the yield stress, typically for too large drop volumes, the drop starts to flow over the plane, in that case it now significantly spreads. We did not study this case.

Figure 14 shows that generally the curves of displacement vs time have a slope 1 in log–log scale, meaning that a steady motion has been reached. In that case, we can consider that wall slip occurs, since we have a constant motion of the rigid bulk along the wall. For too small angles of inclination or volumes, the curve slope may slowly decrease and finally, the sample stops moving at long time (see Fig. 14). This is a situation similar to that of the deformation then stoppage of a sample in rheometrical tests for a stress lower than the slip yield stress. Here, the edge effects (side deposits) might again be at the origin of this effect. However, the critical stress associated with edge effects is more difficult to determine than in rheometry. Indeed, here the additional friction associated with some fluid flow at the edge acts over a fraction of the perimeter which may vary from one test to another depending on the sample shape, which in addition may vary slightly due to some sample deformation during the flow initiation. As a consequence, for the inclined plane tests, we simply represent the wall slip velocity as a function of the total stress (and not after withdrawing some residual value). We did the same for tests with a Teflon-coated surface. Besides, note that with the silicon wafer we varied the drop shape in some tests, which did not appear to change the results in terms of slip law.

It appears that the data obtained at relatively high stress (typically larger than 5 Pa) again fall along slope 1 (see Fig. 15) and are similar to the data obtained from rheometrical tests. This demonstrates that the process at the origin of wall slip when the fluid is constrained between two solid surfaces works in the same way under unconfined conditions. At smaller stress, say for $\tau < 5$ Pa, some deviations from this law appear, which is likely due to the impact of the slip yield stress not taken into account here (see above).

In order to get more insight into this process, we carried out the same test [with emulsion B (82%)] but now after

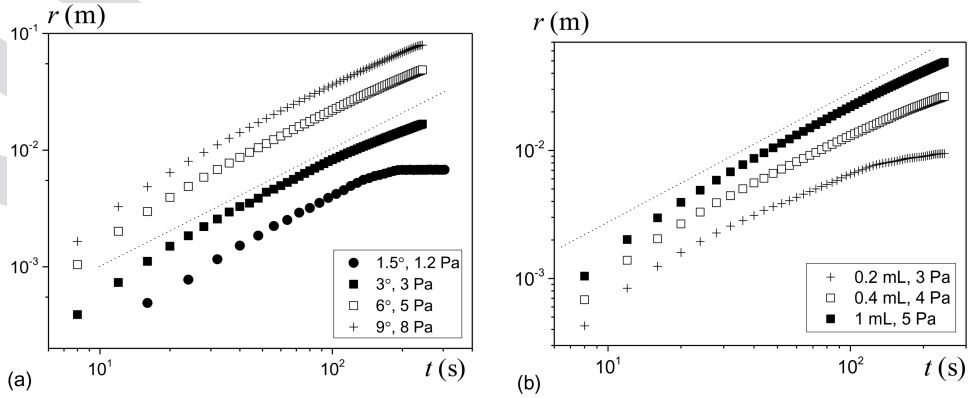

FIG. 14. Tests over smooth inclined planes with emulsion B (82%): position vs time for (a) different angles of inclination (for a volume of 1 ml) and (b) different sample volumes (for an angle of inclination of 6°). The corresponding wall shear stress is indicated in the caption. Dotted lines of slope 1 are showed in both figures as guides for the eyes.

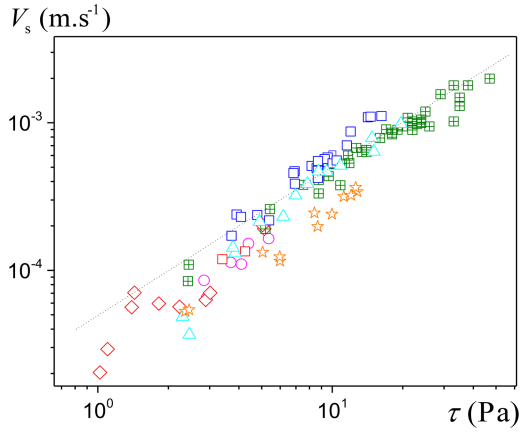

FIG. 15. Slip velocities of emulsion B (82%) in the steady state motion over smooth inclined plane surface, for various drop volumes and surfaces: 0.2 ml (pink circles); 0.4 ml (red diamonds); 1 ml (green cross-squares); 2 ml (blue squares); 1 ml on a Teflonlike coated surface (light blue triangles); and 1 ml on a silicone oil covered surface (orange stars). The dotted line is the slip model fitted to the direct emulsions at different concentrations [see Fig. 8(a)].

having covered the smooth plane by a thin layer of oil (viscosity 0.35 Pa s). The thickness of this layer could not be controlled, and it continuously decreased in time during the test, as the oil flowed downward, but it is order of a few hundreds of micrometers when the emulsion drop is placed above it. However, this does not affect our qualitative observations: as the sample moves downward it seems to "clean" the plane, i.e., there does not seem to be oil behind the sample along its path; the slip velocity is not significantly affected by the presence of this oil layer: it is about two times smaller than without oil (see Fig. 15).

Under these conditions, considering that there remains an oil layer of thickness of the same order as the usual slip layer, due to the much larger viscosity of the oil, its contribution to slip will be much weaker (for the same stress) than that of water, and we can conclude that wall slip is still governed by a slip layer roughly similar to the standard one (without oil).

More surprising is the removal of the oil layer between the emulsion and the wall. Indeed, as a first approximation, we can describe the process as the squeeze flow of a fluid layer between two disks of radius R situated at a distance b and approached to each other with a normal force F. This normal force is the sample weight, i.e., typically 0.01 N. Following the lubrication assumption (see [2]), we can compute the velocity of approach, $V = 8Fb^3/3\pi\mu R^4$. For an initial distance b of the order of 300 μm, we find $V \approx 0.5\,\mu\mathrm{m\,s^{-1}}$, which could explain the disappearance of the oil layer over the test duration (typically 100 s), but as long as b decreases V strongly decreases so that it is already 1000 times smaller for $b = 30\,\mu$m. This means that the oil layer cannot be removed by this simple effect. This suggests that there is a kind of attraction between the elements (droplets) of the material and the solid surface, which tends to further push away the oil. This implies that in any case, some droplets will be positioned at a very short distance from the wall, and this effect plays a critical role in wall slip.

G. Wall slip beyond yielding

Our different techniques above limit the wall slip measurements to the slip regime, where the bulk remains in its solid regime. We used NMR velocimetry to probe the slip velocity when the bulk material is flowing, either in a capillary or in a Couette cell.

Typical velocity profiles obtained in the capillary are shown in the inset of Fig. 16. The integration of each profile is in quantitative agreement with the corresponding flow rate. As expected from the shear stress decrease from the wall to zero along the central axis, the material is essentially sheared near the wall, while the central region remains unsheared, indicating that the shear stress τ is now below τ_c. We estimate the slip velocity V_s from the intersection of the wall and the profile extrapolated to the wall. The uncertainty (shown by error bars) comes from the uncertainty on the exact position of the wall and the dispersion of data point at the approach of the wall. Besides, as we could not obtain at the same time reliable measurement of the pressure drop inside the capillary, the shear stress τ along the wall is estimated from the shear rate value observed along the wall by using the constitutive equation measured independently through standard rheometry.

The corresponding values for V_s and τ are reported in Fig. 16 along with the data obtained from rheometry. The data for different capillary diameters are consistent though scattered. Although they correspond to stress values significantly larger than the yield stress, they seem to be in continuity with the effect of a faster increase of the slip velocity at the approach of the yield stress, and the data appear to approximately follow a quadratic variation.

Data with a Couette cell allow a more complete view of the evolution of flow characteristics as the velocity is increased. At sufficiently low rotation velocity of the inner cylinder (i.e., $V < 0.4$ cm/s), we do not observe any significant shear of the material: essentially, there is an approximately similar slip velocity along both walls, and the velocity

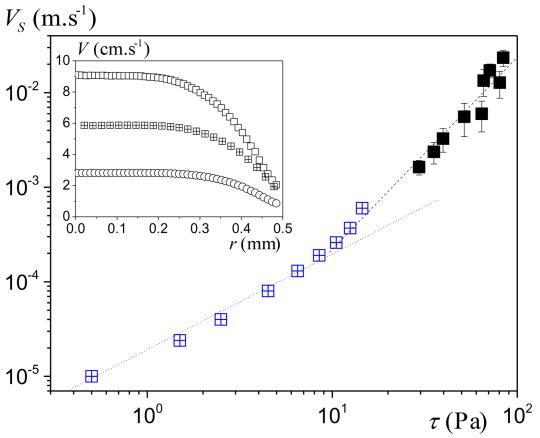

FIG. 16. Slip velocity deduced from velocity profiles in capillaries (black symbols) and deduced from rheometrical tests (blue cross-squares) as a function of the shear stress, for an inverse emulsion (74%). Straight lines of slope 1 (dotted) and 2 (dashed) in log–log scale are plotted as a guide for the eye. The inset shows a set of typical velocity profiles for different flow rates (from bottom to top, 1, 2, and 3 ml/min) in a 1-mm diameter tube.

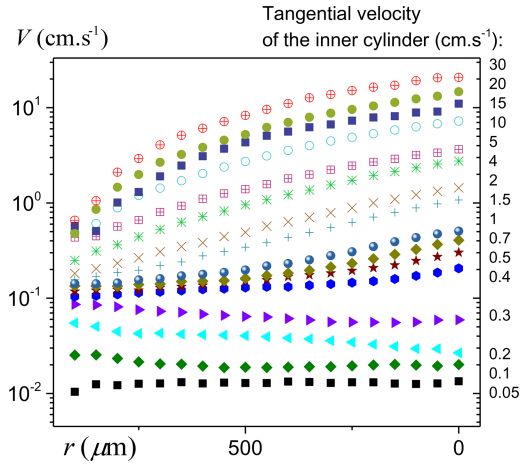

FIG. 17. The NMR velocity profile for the inverse emulsion (82%) in the Couette geometry: tangential velocity as a function of the distance from the inner cylinder wall, for different tangential velocities of the inner cylinder.

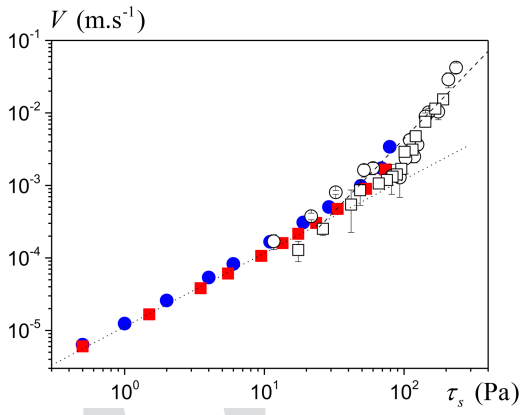

FIG. 18. Slip velocity deduced from the velocity profiles in the Couette cell (open symbols) as a function of the stress, for an inverse emulsion (82%), and from parallel plate tests in rheometer (filled symbols) along a glass surface (squares) or a PMMA surface (circles). Straight lines of slope 1 (dotted) and 2 (dashed) in log–log scale are plotted as a guide for the eye.

profile is a plateau (see Fig. 17). Note that in the slip regime, the material turns as a plug with a rotation velocity Ω so that the tangential velocity in the bulk slightly increases from Ωr_1 along the inner cylinder to Ωr_2 along the outer cylinder, which leads to a total increase by a factor about 1.1 in our case. Here, in some cases, we observe a (nonphysical) more significant increase of the velocity toward the outer cylinder which *a priori* reflects the uncertainty on NMR measurements. For larger rotation velocities, the evolution of the velocity profiles is completely different: there is now a sheared region along the inner wall, which grows in size as the velocity is increased, while the unsheared region progressively disappears; at the same time, there is still some wall slip along each wall (see Fig. 17), which may be appreciated from the difference between the last value in the profile and the wall velocity (indicated in the graph).

We can now compare the slip velocity observed in the Couette cell from NMR measurements with those deduced from rheometry in the nonyielding regime. This is done by extracting the slip velocity (at both walls) from the profiles and associate them with the stress along each wall deduced from the torque measured from independent similar rheometrical tests with the same geometry in a rheometer. We see that the slip velocity observed in both cases in the nonyielding regime (at the approach of the yield stress) are consistent (see Fig. 18), although here the smooth surfaces are made of PMMA and glass. In this regime, we again observe the linear variation of the velocity with the stress, but at the approach of the yield stress value the velocity increases faster, apparently faster than a quadratic law (see Fig. 18). This confirms the results obtained in the capillary and suggests a change of regime and physical process for wall slip when the yield stress fluid is sheared along the wall.

V. ANALYSIS

Let us now review the different results obtained and interpret them in terms of physical origin of wall slip.

1. The wall slip yield stress on smooth surfaces may have two origins: either an edge effect enhanced by evaporation along the line of contact at the sample periphery, or some adhesion between the suspended elements and the solid wall. Usually, edge effects induce a wall slip yield stress of a maximum of a few Pascals, and which tends to increase after some rest.
2. Surface effects were observed with inverse emulsions. In that case, the critical stress associated with adhesion, i.e., τ_c', is very sensitive to the exact surface characteristics.
3. From our experiments, it appears that surface effects appear with inverse emulsions on hydrophilic surface and

TABLE I. Compositions, methods of preparation, and characterization of emulsions used in this work.

Emulsion name	Dispersed phase	Continuous phase	Concentration (vol. %)	Surfactant	Emulsifier	Max. rotation speed (rpm)	Mean droplet size in μm (polydispersity in brackets)
A1	Silicone oil	Water (50 wt. %) and	82	TTAB	Couette	600	3.2 (0.8) or 3.4 (0.7)
A2		glycerol (50 wt. %)				300	4 (0.6)
A3						150	11 (0.8)
A4					Silverson	6000	1.1 (1.6)
A5						2400	2.3 (0.7)
B	Dodecane oil	Water	72–92	SDS		6000	2 (0.4) for the concentration of 82 vol. %
Inverse emulsions	Water and $CaCl_2$	Dodecane oil	72–86	SMO			Not characterized

TABLE II. Surfaces and contact angles of different liquids.

Surface name	Roughness	Contact angle in ° with 5° uncertainty		
		Silicone oil drop surrounded by water/ glycerol mixture with 3 wt. % TTAB	Dodecane drop surrounded by water with 3 wt. % SDS	Water drop with $CaCl_2$ surrounded by dodecane oil with 7.5 wt. % SMO
Silicon	Below 0.3 nm	≈0	≈0	24
Silicon with teflon coating	Below 10 nm	Not measured	≈0	21
Black Silicon	About 6 μm	Not measured	≈0	Not measured

are enhanced (or appear, with direct emulsions) with hydrophobic surface. This suggests that it is due to the attraction and direct contact of water droplets with the wall for hydrophilic surface. We, nevertheless, have no clear explanation for the stronger adhesion effect observed with Teflonlike surface for both types of emulsions.

4. In any case, when τ_c' is removed from the stress, the resulting relationship between stress and slip velocity is linear, as long as the stress is below the yield stress. This relationship appears to apply to a wide range of materials including a variety of structures, element characteristics, and concentrations [23]. In particular, there is no significant impact of the element size, i.e., no clear impact when the droplet size is increased by 1 order of magnitude. And there is no clear impact of the concentration of elements, i.e., no clear impact when the concentration is increased from 72% to 92%, which means that the porosity is decreased by a factor about 4. Moreover, for this range of materials, the apparent liquid layer thickness remains in a rather narrow range, i.e., 35 ± 15 nm. Nevertheless, for inverse emulsions, for which τ_c' could be clearly associated with surface effects, this range is lower: 20 ± 10 nm.
5. This relationship, established for flows inside the geometry of a rheometer, remains valid for flows in the capillary and for unconfined flows, i.e., free surface flows. Thus, for applications, the wall slip law determined from rheometrical tests can be used for describing wall slip of the same material under various other flow conditions as long as the solid surface is sufficiently smooth.
6. In particular, this wall slip law is independent of the normal force applied to the sample, as long as this force does not induce an elongational flow of the material, i.e., as long as the material does not yield. When some elongational flow is induced, a wall slip effect can still occur, with now an apparent liquid layer of thickness several orders of magnitude larger than that for simple shear (see [46]).
7. Experiments of direct emulsion motion over inclined plane, initially covered with oil, show that wall slip then occurs under the same condition, meaning that the material tends to push away the oil layer to reach conditions around the interface similar to those without oil.
8. For a stress larger than the yield stress, the slip velocity appears to increase with the stress faster than below the yield stress, approximately with the square of the shear stress. This is in agreement with previous observations with Carbopol gels [47] and emulsions [48]. However, the general scaling with a power of $\tau - \tau_c$ suggested by Divoux *et al.* [49] for microgels, although it might apply, cannot here be tested relevantly because of the scattering on our data.
9. The wall slip characteristics are significantly modified with a wall exhibiting a roughness of the order of the droplet size. There is now a significant slip yield stress not due to edge effects, but the additional stress needed for wall slip beyond that point is smaller than with smooth surfaces.

The simplest way to interpret the linear relationship for the slip stress as a function of the slip velocity and its proportionality with the interstitial liquid viscosity is to consider that a uniform and constant liquid layer (of thickness δ) exists between the wall and the bulk (i.e., the homogeneous mixture of elements and liquid). However, such a uniform layer is unrealistic considering the disordered and heterogeneous systems we are dealing with. More likely, we can expect that some elements are closer than others from the wall. It was suggested [24] that, since the suspended elements are jammed in some structure, at the origin of the yield stress, this structure exhibits a roughness, and there is a wide range of distances between the elements along this surface and the wall. This implies that the thickness δ would in fact represent an average apparent thickness. For example, if we assume that the liquid is simply sheared between all the element points and the wall, the mean stress is found by averaging the local resulting force$\mu(V_s/\delta_i)ds_i$ over the surface. Then, the apparent liquid layer thickness is $S\left(\sum_i (1/\delta_i)ds_i\right)^{-1}$. In this context, the points for which δ_i is the smallest play a major role. This was already identified by Princen [23], who in fact provided a complete approach of the problem for a relatively simple material, i.e., emulsions. Princen [23] showed that we should expect a fraction of droplets only, squeezed against the wall but separating from it by flat liquid films. In this frame, Princen neglected the impact of the flow of the liquid situated besides, which was considered as "deep oceans" as compared to these films. In the above theoretical approach, this means that δ_i in these regions is more than 1 order of magnitude larger than in the films, which seems realistic if we compare the value we found for δ, typically a few tens of nanometers, to the typical pore size in our emulsions which should be larger than a few hundreds of nanometers. Moreover, in the absence of variation of other aspects, this assumption would be consistent with the observation that the droplet size has no significant impact on wall slip characteristics, since in that case, the pore size varies proportionally to the droplet size. Finally, this

leads to $\delta \approx \delta_0/f$, in which δ_0 is the thickness of the films, and f the fraction of surface occupied by the films.

From direct measurements, Princen found that f varies from about 0.02 for $\phi = 72\%$ to about 0.26 for $\phi = 92\%$. Assuming a constant value for δ_0, this should lead to a decrease of δ by a factor 13 in this range of concentrations. This is in total disagreement with our data (and those of Princen, even if he did not withdraw the apparent slip yield stress), we essentially find no impact of the concentration of the emulsion. Note that this problem is not immediately solved by taking into account a possible variation of δ_0 due to the variation of osmotic pressure with the concentration, as to maintain a constant δ, we would need here an increase of δ_0 for an increase of the osmotic pressure, in contradiction with the natural expectation in the absence of other effects.

On the other side, if we now just consider the standard models assuming a balance between attractive and repulsive forces (see above), it is remarkable that for our emulsions, according to proposed estimations [41,43], we expect variations of the osmotic pressure by a factor of several tens when increasing the emulsion concentration between 72% and 92%, whereas we did not notice any impact of concentration on the apparent slip thickness. This suggests that the slip layer thickness is imposed by some effect stronger than the stress resulting from the jamming of the elements.

However, we have also seen that beyond that point, i.e., for a stress larger than the yield stress and thus leading to an elongational flow, the wall slip characteristics change abruptly: the apparent liquid layer thickness turns to a value several orders of magnitude larger than that for the shear flow below the yield stress (i.e., of the order of 10 μm [42]). This means that in that case there is a kind of irreversible detachment of the elements from the wall, implicitly meaning that they were somehow attached in the previous situation. This kind of attachment is further supported by the inclined plane tests with an initial oil layer, which is apparently removed by the emulsion sample, as if the droplets tended to be attracted by the wall.

This suggests that there are significant van der Waals attractive forces between the droplets and the wall, which leads to push them to be in contact (in fact, at a distance of a few molecules) around some point of their surface. Although we must admit that we cannot fully explain the origin of this effect, such a scheme would explain most observed trends. Indeed, the dominant region of liquid shear would be concentrated around those points situated at a distance of the order of a nanometer. As a counterpart, the area concerned would be rather limited. The resulting apparent liquid layer thickness would vary with the number of contacts, and thus would only slightly vary when the concentration is varied in the range tested. Finally, this scheme would explain that the elements tend to be able to remove at large distance from the wall when some critical force has been applied. In contrast, there should be a significant dependence with the droplet size, since the number of contact points decreases with r^{-3}. Note that we indeed observed an increase in apparent slip layer thickness, but it is much smaller than expected from this approach, possibly due to the large size distributions of our samples.

Under these conditions, a change in the wall slip properties will occur when one applies some sufficiently large stress to extract the elements from the wall, i.e., move them at such a distance that the attractive force is now negligible. In that case, the elements would move at a much larger distance from the wall over some distance and possibly get back to it. This would reduce the stress needed to get wall slip, thus explaining the increase in slip velocity (or equivalently the increase of apparent slip layer thickness) observed for all materials (see Figs. 9, 13, and 18) at the approach of the yield stress. This process would tend to develop further, with more and more elements detached from the wall, or equivalently spending more time detached, as the stress further increases, which might explain the transition to a new regime of variations of slip velocity with stress at large stresses (see Fig. 18). When this regime is well developed we can consider that all elements remain detached from the wall so that their mean distance from the wall could now result from a balance between some lubrication effect and osmotic effect, as assumed in the Meeker *et al.* model [11], thus leading approximately to a quadratic variation.

With a surface of roughness of the order of the element size, the elements can also be jammed in the wall structure, from which they can be extracted thanks to a stress larger than a critical value, as for a friction between two solid surfaces. This explains the appearance of a finite wall slip yield stress in that case. This effect was described in detail in the case of bubbles moving along a rough plane (see [49]). Then the droplets can move along the surface but the contacts with the solid surface are now more seldom, as they have to jump from one contact to another on successive peeks of the roughness. This explains that the (additional) stress *a priori* solely due to lubrication in the total slip stress is smaller than that for a smooth surface for which the contact is maintained. Finally, with such a slightly rough surface, it appears possible to still obtain some wall slip, but now with two opposite effects: a wall slip yield stress, which must be overcome for the flow initiation, and a larger apparent wall slip layer associated with motion beyond this yielding. This means that we have a kind of aquaplanning effect, in which the elements, after being extracted from the roughness, now encounter a smaller resistance to motion than with a smooth wall.

VI. CONCLUSION

The above results finally provided some clues about the physical explanations of wall slip mechanisms, but they also essentially give us a general view of the wall slip characteristics. Indeed, if we generalize these results obtained with different model materials and some complex materials (from [23]), different surfaces and different flow conditions, we get the following picture:

- Pure wall slip (without bulk flow) is observed for a stress between a wall slip yield stress and the material yield stress.
- The value of this wall slip yield stress is thus critical, as it determines the ability of a given material volume material to slip over a solid surface, depending on the surface of contact between the material and the solid.

- This wall slip yield stress may be essentially due to edge effects.
- Alternatively, it may find its origin in some adhesion between the material elements (composing the jammed structure of the yield stress fluid) and the solid surface, or some adherence due to the roughness of the surface.
- Wall slip (below the yield stress) disappears when the adhesion or adherence leads to a wall slip yield stress expected to be larger than the material yield stress.
- The stress minus the wall slip yield stress is generally proportional to the slip velocity so that wall slip may be described (even if the reality is likely more complex) as due to the shear of an interstitial liquid layer of given thickness.
- Whatever the material type, the thickness of this layer appears to vary in a rather narrow range, typically around a few tens of nanometers.
- At the approach of the yield stress, the wall slip properties change, the velocity now tending to increase faster with the stress.
- Beyond the yield stress slip still apparently occurs, but now the slip velocity clearly varies with a power of the stress typically of the order of 2.
- This suggests that wall slip has a different nature in this regime, it now likely involves both an interstitial liquid flow and the displacement of elements unjammed from the bulk.

Further work remains to be done to understand the exact properties at the origin of the adhesion on the solid surface below the yield stress and to understand the exact processes at work for wall slip beyond the yield stress.

ACKNOWLEDGMENT

We acknowledge the fruitful discussions with Michel Cloitre and Marie le Merrer.

APPENDIX

Tables I and II provide ■.

References

[1] Liu, A. J., and S. R. Nagel, "Nonlinear dynamics: Jamming is not just cool any more," Nature **396**, 21–■ (1998).

[2] Coussot, P., *Rheometry of pastes, suspensions, and granular materials: Applications in industry and environment* (Wiley, New York, 2005).

[3] Barnes, H. A., "A review of the slip (wall depletion) of polymer solutions, emulsions and particle suspensions in viscometers: Its cause, character, and cure," J. Nonnewtonian Fluid Mech. **56**, 221–251 (1995).

[4] Granick, S., Y. Zhu, and H. Lee, "Slippery questions about complex fluids flowing past solids," Nat. Mater. **2**, 221–227 (2003).

[5] Stokes, J. R., M. W. Boehm, and S. K. Baier, "Oral processing, texture and mouthfeel: From rheology to tribology and beyond," Curr. Opin. Colloid Interface Sci. **18**, 349–359 (2013).

[6] Ozkan, S., T. W. Gillece, L. Senak, and D. J. Moore, "Characterization of yield stress and slip behaviour of skin/hair care gels using steady flow and LAOS measurements and their correlation with sensorial attributes," Int. J. Cosmet. Sci. **34**, 193–201 (2012).

[7] Chen, L., Y. Duan, C. Zhao, and L. Yang, "Rheological behavior and wall slip of concentrated coal water slurry in pipe flows," Chem. Eng. Proc. Process Intensif. **48**, 1241–1248 (2009).

[8] Ngo, T. T., E. H. Kadri, R. Bennacer, and F. Cussigh, "Use of tribometer to estimate interface friction and concrete boundary layer composition during the fluid concrete pumping," Constr. Build. Mater. **24**, 1253–1261 (2010).

[9] Rungraeng, N., S. H. Yoon, Y. Li, and S. Jun, "Development of a self-slippery liquid-infused porous surface (SLIPS) coating using carbon nanotube composite for repelling food debris and microbial biofilms," Trans. ASABE **58**, 861–867 (2015).

[10] Salmon, J. B., S. Manneville, A. Colin, and B. Pouligny, "An optical fiber based interferometer to measure velocity profiles in sheared complex fluids," Eur. Phys. J. Appl. Phys. **22**, 143–154 (2003).

[11] Meeker, S. P., R. T. Bonnecaze, and M. Cloitre, "Slip and flow in pastes of soft particles: Direct observation and rheology," J. Rheol. **48**, 1295–1320 (2004).

[12] Manneville, S., L. Bécu, and A. Colin, "High-frequency ultrasonic speckle velocimetry in sheared complex fluids," Eur. Phys. J. Appl. Phys. **28**, 361–373 (2004).

[13] Callaghan, P. T., "Rheo-NMR: Nuclear magnetic resonance and the rheology of complex fluids," Rep. Prog. Phys. **62**, 599–670 (1999).

[14] Loppinet, B., J. K. G. Dhont, and P. Lang, "Near-field laser Doppler velocimetry measures near-wall velocities," Eur. Phys. J. E **35**, 62–■ (2012).

[15] Cloitre, M., and R. T. Bonnecaze, "A review on wall slip in high solid dispersions," Rheol. Acta **56**, 283–305 (2017).

[16] Meeker, S. P., R. T. Bonnecaze, and M. Cloitre, "Slip and flow in soft particle pastes," Phys. Rev. Lett. **92**, 198302 (2004).

[17] Seth, J. R., M. Cloitre, and R. T. Bonnecaze, "Influence of short-range forces on wall-slip in microgel pastes," J. Rheol. **52**, 1241–1268 (2008).

[18] Denkov, N. D., V. Subramanian, D. Gurovich, and A. Lips, "Wall slip and viscous dissipation in sheared foams: Effect of surface mobility," Colloids Surf. A Physicochem. Eng. Asp. **263**, 129–145 (2005).

[19] Le Merrer, M., R. Lespiat, R. Höhler, and S. Cohen-Addad, "Linear and non-linear wall friction of wet foams," Soft Matter **11**, 368–381 (2015).

[20] Ballesta, P., R. Besseling, L. Isa, G. Petekidis, and W. C. K. Poon, "Slip and flow of hard-sphere colloidal glasses," Phys. Rev. Lett. **101**, 258301 (2008).

[21] Ballesta, P., G. Petekidis, L. Isa, W. C. K. Poon, and R. Besseling, "Wall slip and flow of concentrated hard-sphere colloidal suspensions," J. Rheol. **56**, 1005–1037 (2012).

[22] Princen, H. M., "Rheology of foams and highly concentrated emulsions—II. Experimental study of the yield stress and wall effects for concentrated oil-in-water emulsions," J. Colloid Interface Sci. **105**, 150–171 (1985).

[23] Zhang, X., E. Lorenceau, P. Basset, T. Bourouina, F. Rouyer, J. Goyon, and P. Coussot, "Wall slip of soft-jammed systems: A generic simple shear process," Phys. Rev. Lett. **119**, 208004 (2017).

[24] Nguyen, T. T. L., Micromechanical approach of the behavior of bubble suspension in a yield stress fluid, Ph.D. thesis, Univ. Paris-Est, Champs sur Marne, France, 2015 (in French).

[25] Chevalier, T., C. Chevalier, X. Clain, J. C. Dupla, J. Canou, S. Rodts, and P. Coussot, "Darcy's law for yield stress fluid flowing through a porous medium," J. Nonnewton. Fluid Mech. **195**, 57–66 (2013).

[26] Princen, H. M., and A. D. Kiss, "Rheology of foams and highly concentrated emulsions: IV. An experimental study of the shear viscosity and yield stress of concentrated emulsions," J. Colloid Interface Sci. **128**, 176–187 (1989).

[27] Shive, L. W., and B. L. Gilmore, "Impact of thermal processing on silicon wafer surface roughness," ECS Trans. **16**, 401–405 (2008).

[28] Jansen, H., M. de Boer, R. Legtenberg, and M. Elwenspoek, "The black silicon method: A universal method for determining the parameter setting of a fluorine-based reactive ion etcher in deep silicon trench etching with profile control," J. Micromech. Microeng. **5**, 115–120 (1995).

[29] Nguyen, K. N., P. Basset, F. Marty, Y. Leprince, and T. Bourouina, "On the optical and morphological properties of microstructured Black Silicon obtained by cryogenic-enhanced plasma reactive ion etching," J. Appl. Phys. **113**, 194903 (2013).

[30] Dorrer, C., and J. Rühe, "Silicon nanograss: From superhydrophilic to superhydrophobic surfaces," Adv. Mater. **20**, 159–163 (2008).

[31] Saab, D. A., P. Basset, M. J. Pierotti, M. L. Trawick, and D. E. Angelescu, "Static and dynamic aspects of black silicon formation," Phys. Rev. Lett. **113**, 265502 (2014).

[32] Lafuma, A., and D. Quéré, "Superhydrophobic states," Nat. Mater. **2**, 457–460 (2003).

[33] Marmur, A., "The lotus effect: Superhydrophobicity and metastability," Langmuir **20**, 3517–3519 (2004).

[34] Fukushima, E., "Nuclear magnetic resonance as a tool to study flow," Ann. Rev. Fluid Mech. **31**, 95–123 (1999).

[35] Callaghan, P. T., *Principles of Nuclear Magnetic Resonance Microscopy* (Oxford Science, Oxford, 1991).

[36] Yunker, P. J., T. Still, M. A. Lohr, and A. G. Yodh, "Suppression of the coffee-ring effect by shape-dependent capillary interactions," Nature **476**, 308–311 (2011).

[37] Seth, J. R., C. Locatelli-Champagne, F. Monti, R. T. Bonnecaze, and M. Cloitre, "How do soft particle glasses yield and flow near solid surfaces," Soft Matter **8**, 140–148 (2012).

[38] Mansard, V., L. Bocquet, and A. Colin, "Boundary conditions for soft glassy flows: Slippage and surface fluidization," Soft Matter **10**, 6984–6989 (2014).

[39] Derzsi, L., D. Filippi, G. Mistura, M. Pierno, M. Lulli, M. Sbragaglia, M. Bernaschi, and P. Garstecki, "Fluidization and wall slip of soft glassy materials by controlled surface roughness," Phys. Rev. E **95**, 0526202 (2017).

[40] Paredes, J., N. Shahidzadeh, and D. Bonn, "Wall slip and fluidity in emulsion flow," Phys. Rev. E **92**, 042313 (2015).

[41] Mason, T. G., M. D. Lacasse, G. S. Grest, D. Levine, J. Bibette, and D. A. Weitz, "Osmotic pressure and viscoelastic shear moduli of concentrated emulsions," Phys. Rev. E **56**, 3150–3166 (1997).

[42] Zhang, X., O. Fadoul, E. Lorenceau, and P. Coussot, "Yielding and flow of soft-jammed systems in elongation," Phys. Rev. Lett. **120**, 048001 (2018).

[43] Maestro, A., W. Drenckhan, E. Rio, and R. Höhler, "Liquid dispersions under gravity: Volume fraction profile and osmotic pressure," Soft Matter **9**, 2531–2540 (2013).

[44] Coussot, P., S. Proust, and C. Ancey, "Rheological interpretation of deposits of yield stress fluids," J. Nonnewton. Fluid Mech. **66**, 55–70 (1996).

[45] Roussel, N., and P. Coussot, ""Fifty-cent rheometer" for yield stress measurements: From slump to spreading flow," J. Rheol. **49**, 705–718 (2005).

[46] Salmon, J. B., L. Bécu, S. Manneville, and A. Colin, "Towards local rheology of emulsions under Couette flow using dynamic light scattering," Eur. Phys. J. E **10**, 209–221 (2003).

[47] Géraud, B., L. Bocquet, and C. Barentin, "Confined flows of a polymer microgel," Eur. Phys. J. E **36**, 30–■ (2013).

[48] Divoux, T., V. Lapeyre, V. Ravaine, and S. Manneville, "Wall slip across the jamming transition of soft thermoresponsive particles," Phys. Rev. E **92**, 060301 (2015).

[49] Germain, D., and M. Le Merrer, "Bubbles slipping along a crenetaled wall," Eur. Phys. Lett. **115**, 64005 (2016).